Available online at www.sciencedirect.com

ScienceDirect

materialstoday: PROCEEDINGS

Materials Today: Proceedings 2 (2015) 637 – 646

12th European Conference on Thermoelectrics

Volume texture and anisotropic thermoelectric properties in $Ca_3Co_4O_9$ bulk materials

Driss Kenfaui[a,b]*, Daniel Chateigner[b], Moussa Gomina[b], Jacques G. Noudem[b], Bachir Ouladdiaf[c], Anne Dauscher[a], Bertrand Lenoir[a]

[a] *Institut Jean Lamour, UMR 7198 CNRS-Université Lorraine, Parc de Saurupt, 54011 Nancy, France*
[b] *CRISMAT, UMR 6508 CNRS/ENSICAEN, LUSAC, Université de Caen Basse-Normandie, 6 Bd Maréchal Juin, 14050 CAEN Cedex 04, France*
[c] *Institut Laue-Langevin (ILL), 6 rue J. Horowitz, BP 156-38042 Grenoble, Cedex 09, France*

Abstract

$Ca_3Co_4O_9$ lamellar thermoelectric (TE) oxides are potentially suitable for energy conversion applications at high temperature in air. To be used in TE devices, bulk $Ca_3Co_4O_9$ materials must possess large texture strengths to attain the optimal TE performances, and sufficient material size to fabricate TE ceramic elements (legs). This paper reports the development of thick $Ca_3Co_4O_9$ multilayer samples by hot-pressing a stack of dense and strongly textured $Ca_3Co_4O_9$ bulk single-layer samples along their mean **c***-axis. The volume texture was investigated by using the neutron diffraction method, and revealed the largest strength achieved hitherto in such materials. The Seebeck coefficient, S, electrical resistivity, ρ, and thermal conductivity, κ, were determined parallel (S^c, ρ^c, κ^c) and perpendicular (S^{ab}, ρ^{ab}, κ^{ab}) to the mean **c***-axis. ρ and κ were found to be highly anisotropic, with ratios $\rho^c/\rho^{ab} = 8.8$ and $\kappa^{ab}/\kappa^c = 2.7$ at 900 K, respectively. S unexpectedly depicted an anisotropic character as well, but it remains less prominent. The power factor, PF, and figure-of-merit, ZT, were hence anisotropic, exhibiting respective ratios $PF^{ab}/PF^c = 12$ and $ZT^{ab}/ZT^c = 4.6$. The ZT^{ab} value reached 0.16 at 900 K which is 2 fold the one of conventionally sintered materials.

Selection and peer-review under responsibility of Conference Committee members of the 12th European Conference on Thermoelectrics.

Keywords: $Ca_3Co_4O_9$ thermoelectric oxides; neutron diffraction; texture; thermoelectric properties; figure of merit; anisotropy.

* Corresponding author: D. Kenfaui; Tel.: +33 659 302 892.
E-mail address: driss.kenfaui@univ-lorraine.fr

2214-7853 © 2015 Published by Elsevier Ltd.
Selection and peer-review under responsibility of Conference Committee members of the 12th European Conference on Thermoelectrics.
doi:10.1016/j.matpr.2015.05.089

1. Introduction

Layered cobalt oxides $Ca_3Co_4O_9$ are considered to be among the most expected material candidates for thermoelectric (TE) energy conversion applications at high temperature because they possess fairly good TE properties, resist oxidation in air, are thermally and chemically stable even up to 1200 K, and do not exhibit any polluting or toxic character [1-4]. They were indeed reported with high Seebeck coefficient, *S*, concomitant with relatively low resistivity, ρ, and thermal conductivity, κ, in their in-plane (i.e. (**a**,**b**) planes), thereby leading to a good TE conversion efficiency dictated by the dimensionless figure-of-merit $ZT = (S^2 \mathrm{x} T)/(\rho \mathrm{x} \kappa)$ of 0.3-0.4 at 950-1100 K [1], where T refers to the absolute temperature. The $Ca_3Co_4O_9$ crystal structure consists of CdI_2-type hexagonal CoO_2 layers and NaCl-type Ca_2CoO_3 ones alternatively stacked along the **c**-axis [4]; the $Ca_3Co_4O_9$ phase is hence a composite crystal with **b**-axis lattice misfit. The resulting layered structure would cause a strong TE properties anisotropy which was evidenced for the resistivity [4, 6-10], but not yet for the Seebeck coefficient which is too often considered by the scientific community as an isotropic property despite the crystal structure, even though its anisotropic character has been already predicted by the mean of the asymmetric 3 x 3 tensors [11].

$Ca_3Co_4O_9$ single crystals are less likely to be well-suited for being used in TE devices because they will be too expensive on the one hand, and cannot hitherto be grown in a large size on the other hand. A single crystal shaped as TE elements 'legs' appears practically impossible to elaborate. It is therefore highly desirable to achieve sufficient TE conversion efficiency in a polycrystalline form of such oxides. Bulk materials nevertheless depict low *ZT* values when being fabricated by using the conventional sintering (CS) [1, 9]. Several methods (Spark Plasma Sintering (SPS), Spark Plasma Texturing (SPT), Hot Pressing (HP), Reactive Template Growth (RTG)...) [7-10, 12-15] have been hence explored to process the $Ca_3Co_4O_9$ materials in an effort to minimize current flow barriers and, subsequently, reduce (**a**,**b**) plane electrical resistivity, ρ^{ab}. In recent works, we have reported [8,9] on the fabrication by hot pressing of dense and strongly textured $Ca_3Co_4O_9$ bulk single-layer samples with a noteworthy (**a**,**b**) plane grain growth, which considerably diminishes the electrical resistivity, ρ^{ab}, and thus boosts the power factor, $PF^{ab} = S^{ab2}/\rho^{ab}$.

The processed single-layer samples are however too thin (thickness below 0.5 mm) to assess all their TE properties in the mean (**a**,**b**) planes and to design TE ceramic elements with dimensions (length and section of at least ~ 5 mm and ~ 4 x 4 mm^2, respectively) [16-20] well-suited for TE devices fabrication.

We have found the way to cope with this challenge by fabricating a thick $Ca_3Co_4O_9$ sample (multilayer) by hot-pressing a stack of strongly textured $Ca_3Co_4O_9$ bulk single-layer samples along their mean **c***-axis. The microstructure and texture features were investigated in the core of the processed thick sample. The electrical properties as well as the thermal ones were measured along two principal directions: parallel and perpendicular to the mean **c***-axis of the multilayer sample. An intensive study was conducted to elucidate the influence of the anisotropy on such properties.

2. Experimental

The fabrication of dense $Ca_3Co_4O_9$ bulk textured materials by using HP process is described in detail elsewhere [8, 9]. The starting precursors $CaCO_3$ and Co_3O_4 were weighed in the proper stoichiometric ratios and mixed in an agate ball mill before being calcined in air at 900°C for 24 h to decompose the carbonates and, subsequently, purify the $Ca_3Co_4O_9$ phase. After regrinding, the powder was uniaxially cold-pressed under 95 MPa into 4 mm thick and 25 mm diameter pellets. Such discs were further treated using the HP process as follows: the pellet was set in a home-made furnace between two 0.125 mm - thick silver sheets to avoid an undesirable reaction with the alumina bearing plates. The sample was then heated up to the dwell temperature of 920°C maintained for 24 h under an uniaxial pressure P_{HP} = 30 MPa. The pressure was removed before cooling in the aim of preventing material cracking. The processed $Ca_3Co_4O_9$ discs had a thickness ≤ 0.5 mm, and depicted microstructural features of dense and strongly textured bulk samples, displaying the largest texture strength achieved hitherto in such bulk materials [8, 9] to our knowledge. A pressure higher than 30 MPa resulted in elaborating thinner samples, impractical for further manipulations.

Thirty dense and strongly textured $Ca_3Co_4O_9$ pellets were cut into ~ 18 x 18 x 0.5 mm^3 parallelepiped single-layer

samples and mirror-polished on their two faces (Fig. 1a); their final thickness was consequently diminished to 0.3-0.4 mm. They were thereafter stacked together along their mean **c***-axis and hot-pressed at 920°C under a moderate uniaxial pressure of 10 MPa for 10 h (Fig.1b). The thickness of the resulting thick sample is about 9 mm (Fig.1b-c). It has to be noted here that the total time of HP processing needed for such elaboration exceeded 1100 h.

Using neutron diffraction, the volume texture was quantitatively investigated on a ~ 8 x 6 x 7 mm^3 parallelepiped specimen cut from the core of the multilayer sample. For that purpose, the 2D curved area position sensitive detector (CAPS) of the D19 beam line of the steady-state reactor at ILL (Institut Laue-Langevin, Grenoble, France) [21] was used. The sample was placed in the Eulerian cradle to allow the usual tilt (χ) and azimuth (φ) angle rotations. Since the CAPS detector spans 30° at once out of the diffractometer scattering plane, only 4 χ and 72 φ orientations of the sample in the cradle were required to cover the entire Orientation Distribution space. The diffraction pattern analysis was carried out in the combined Rietveld-EWIMV formalism [21-23], implemented in the MAUD software [24].

The relative percent density of the bulk $Ca_3Co_4O_9$ materials was computed by comparing the samples density measured *via* the Archimedes method (KERN & Sohn GmbH, Baligen, Germany) to the theoretical one reported for the $Ca_3Co_4O_9$ phase [4]. The microstructure was investigated using a Carl Zeiss (Supra 55, Oberkochen, Germany) Scanning Electron Microscope (SEM).

The temperature dependence of the electrical resistivity, ρ, and Seebeck coefficient, S, was monitored in the 350 - 900 K range using a ZEM-3 apparatus (ULVAC-RIKO, Inc, Japan). These properties are measured on ~ 2 x 2 x 8 mm^3 bars cut parallel (ρ^c, S^c) and perpendicular (ρ^{ab}, S^{ab}) to the applied pressing axis. The thermal diffusivity coefficient D was measured by the laser flash diffusivity method using the LFA 457 MicroFlash™ system (NETZSCH-Gerätebau GmbH, Selb / Germany) on ~ 6 x 6 x 2 mm^3 parallelepiped-shaped specimens, cut also from the core of the thick multilayer sample in the directions parallel (D^{ab}) and perpendicular (D^c) to the applied pressing axis. The thermal conductivity κ was then determined using the equation $\kappa = d \times C_p \times D$, where d refers to the density and C_p the specific heat capacity which was measured by the mean of the thermal analyzer (STA 449 F3 Jupiter®, NETZSCH-Gerätebau GmbH, Selb / Germany).

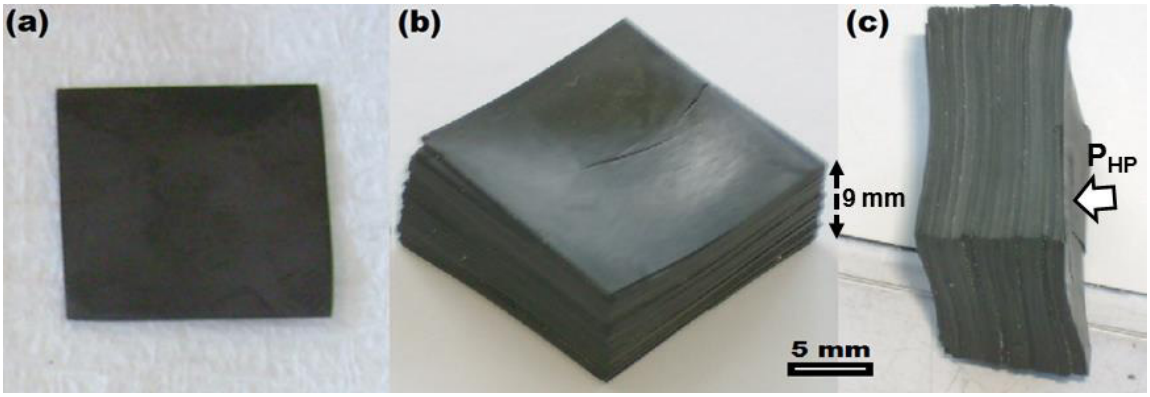

Fig. 1. (**a**) A dense and strongly textured $Ca_3Co_4O_9$ single-layer sample cut into a ~ 18 x 18 x ~ 0.5 mm^3 parallelepiped and polished on its two faces. (**b**) Top view of the thick multilayer sample (18 x 18 x 9 mm^3) fabricated by hot-pressing a stack of thirty single layers. (**c**) Cross section view where the stacked initial layers are visible to the naked eye. The uniaxial pressure was applied parallel to the normal axes of the layers during the HP process as indicated by the arrow.

3. Results and discussion

3.1. Volumic textural characteristics and microstructure

The comparison between the 2D experimental and recalculated neutron diffraction diagrams resulting from Combined Analysis on the parallelepiped-shaped specimen cut from the core of the thick multilayer sample, indicated a good reproducibility between measurements and refinement, with reliability factors Rw = 28.97 %, R_{Bragg} = 21.56 % and R_{exp} = 32.26 % larger than those reported for $Ca_3Co_4O_9$ single-layer samples [8,9]. Such difference is primarily ascribed to the high number of the measurement points on which these factors depend. A Goodness of Fit (GoF) of only 1.8 was reached, which reflects a good global refinement. The resulting refined cell parameters for the thick multilayer sample are a = 4.8510(4) Å, b = 36.361(4) Å and c = 10.8572(5) Å, evidencing a contraction of (**a**,**b**) planes and an extension of those containing the **c**-axis of about 0.0063, 0.165 and 0.0025 Å, respectively, compared to the single-layer sample [8,9]. These $Ca_3Co_4O_9$ structure deformations are probably tied to further HP treatment applied on the stack.

Figure 2 depicts the {020}, {001} and {100} pole figures, reconstructed upon the combined refinement of the orientation distribution function (ODF). The refinement is achieved with reliability factors R_w = 27.53% and R_{Bragg} = 22.87%, in keeping with the high value of the texture strength defined by the texture index [25], F^2 = 27.72 mrd^2. Such values are higher than those attained for the single-layer sample as well (Rw = 1.29%, R_{Bragg}= 2.67% and F^2 = 6 mrd^2) [8, 9]. These pole figures, on the other hand, display a maximum of the {001} poles of around 43 mrd, which is the strongest texture achieved to date in $Ca_3Co_4O_9$ bulk materials, and 2 fold the strength score recorded on the single-layer samples [8, 9].

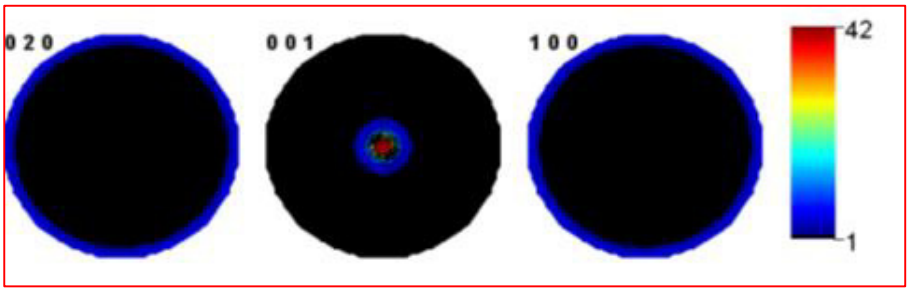

Fig. 2. {020}, {001} and {100} recalculated normalized pole figures for the thick multilayer sample obtained after ODF refinement (linear density scale, equal area projection)

SEM observations of a fractured surface containing the pressing axis (Fig. 3a) revealed a 96%-densified and homogeneous microstructure of the single-layer samples achieved upon HP processing. They depicted indeed a high orientation degree of large grown platelets compactly stacked up along the pressing axis. A surface fractured in a similar direction along the height of the thick multilayer sample (Fig. 3b) showed that the internal alignment of the platelets in the primary single-layer samples was not damaged upon further HP treatment applied to the stack. The microstructure effectively exhibited a similar density and, in particular, platelets strongly aligned along the whole stack height, in coherence with the results obtained from the {020}, {001} and {100} pole figures (Fig. 2).

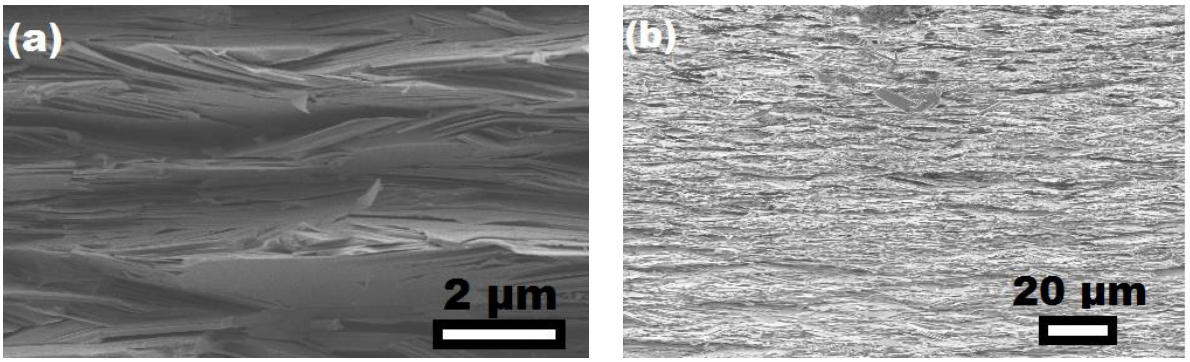

Fig. 3. (a) SEM micrograph of a surface of rupture of a dense and strongly textured $Ca_3Co_4O_9$ single-layer sample processed by HP (30 MPa / 920°C / 24 h). **(b)** The internal alignment of the platelets in the initial single layers inside the thick multilayer sample was not damaged upon further HP treatment applied to the stack.

The orientation distribution (OD), moreover, displayed a maximum value of 121.6 mrd and its minimum was 0, which suggests that all the crystallites are aligned within the same orientation component, or in other words, the <001>* fibre texture with <001>* directions [21] are oriented parallel to the pressing axis of the thick multilayer sample. The inverse pole figure (Fig. 4) determined for the pressing axis (ND) showed that there is actually no other prominent orientation component than the <001>* fibre, and corresponds to levels of orientations along the pressure axis up to 54 mrd.

On the other hand, SEM observations on a mirror-polished section cut parallel to the mean **c***-axis of the thick multilayer sample showed good interfaces between the primary layers, promoting then the microstructural and physical properties homogeneity throughout the whole stack height. The HP process enables then the soldering of the primary layers to each other.

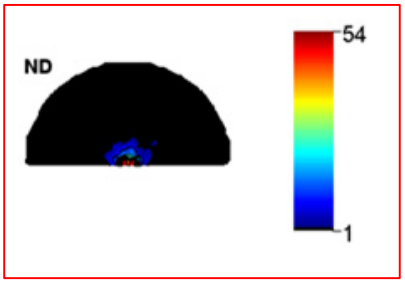

Fig. 4. Inverse pole figure calculated for the direction of the pressure (logarithmic density scale, equal area projection)

It is relevant to note here that the microstructure and texture achieved in the thick multilayer sample exhibit much better characteristics sought for diminishing the ρ^{ab} resistivity compared to those of conventionally sintered $Ca_3Co_4O_9$ bulk sample processed without applied pressure. Indeed, the latter was reported to exhibit a porous microstructure presenting a percent density of only 60% with smaller grains (< 5 µm) which is randomly distributed and loosely assembled [8, 9]. Its maximum of the {001} poles does not exceed 4 mrd. The TE properties of such sample were measured here as well, and compared to those recorded on the thick multilayer one.

3.2. Electrical properties

Figure 5a exhibits the dependence of the electrical resistivity measured in the 300 − 900 K range on four different bars cut parallel, ρ^{c}, and perpendicular, ρ^{ab}, to the mean **c***−axis of the thick multilayer sample. To ease a comparison with the single-layer one, the ρ^{ab} *(T)* curve recorded for the latter is plotted as well. We note a good

reproducibility of the resistivity for both directions, and, in particular, a marked anisotropy evidenced by a large gap between ρ^{ab} (T) and ρ^{c} (T) curves. Such anisotropy can be derived from:

i) The large texture strength which fosters electrical current flow in the (**a**,**b**) planes acts to reduce ρ^{ab}. Indeed, even when the current is injected parallel to the **c***−axis, a part of it circulates in the **(a,b)** planes because a number of them are not exactly perpendicular to the axis of electrical current injection, which makes them contributing partly to the global electrical conductivity in these planes. We cannot, on the other hand, eliminate the ρ^{ac} (i.e. ρ^{13}) tensor component whose value is not *a priori* zero in the $Ca_3Co_4O_9$ monoclinic system [26].

ii) The grain boundary density (GBD) is much lower in the (**a**,**b**) planes than in those containing the mean **c***−axis, due to the noteworthy (**a**,**b**) plane grain growth (≤ 17 µm) concomitant with the thickness reduction of the platelets (≤ 0.12 µm) within the single-layer samples under the effect of hot pressing [8, 9]. That reduces ρ^{ab}, but at the same time causes a strong increase in ρ^{c}.

iii) In the thick multilayer sample, the high number of interfaces between the initial single layers of the stack (Fig.1b-c) limits current flow in the planes containing the mean **c***−axis, inducing then further increase in ρ^{c}.

This results in a high resistivity anisotropy with an average ratio, ρ^{ab}/ρ^{c}, of 8.8 at 900 K, which is similar to that recorded for bulk $Ca_3Co_4O_9$ materials textured by the RTG process [10] and 3 fold the ratio reported for $Ca_3Co_4O_9$ ceramics processed by the SPS method [7].

The resistivity ρ^{ab} of the single-layer sample seems to be similar to that measured in the thick multilayer one, which suggests that the texture strengthening in the latter had not a discernible effect on the current flow in the mean (**a**,**b**) planes. As the texture is a fibre type, the limit of beneficial effect could be seen here as regards the electrical resistivity, if intrinsic anisotropy of crystallites is the sole concern. However, extrinsic harmful effects on resistivity, derived from grain boundaries, still exist, which would require a stronger texture.

In Figure 5b, the temperature dependence of the Seebeck coefficient measured on the same bars, cut parallel, S^{c}, and perpendicular, S^{ab}, to the mean **c***−axis of the thick multilayers sample, is depicted. The $S^{ab}(T)$ curve obtained for the single-layer sample is also given. It shows similar values than those of the thick multilayer sample, whereas the latter presents different S^{ab} and S^{c} evidencing a thermo-power anisotropy in accordance with the asymmetric 3 x 3 tensors description [11]. Since the Seebeck coefficient is represented by 2nd rank tensors [9, 26], it has not been measured as such to our knowledge yet. That means that their anisotropic character has never been experimentally demonstrated, in particular, in strongly textured bulk materials. In a monoclinic crystal system, the Seebeck coefficient tensor is defined with five independent components, S^{M}_{ij}, as:

$$\begin{pmatrix} S_{11} & & S_{13} \\ & S_{22} & \\ S_{31} & & S_{33} \end{pmatrix}$$

However, the macroscopic symmetry allows us to write $S^{M}_{11} = S^{M}_{22}$ and $S^{M}_{13} = S^{M}_{31}$ in the case of the textured bulk materials possessing a <001>* fibre texture; there are then only three independent components, S^{M}_{ij}. Here, we measured two Seebeck coefficient components, $S^{M}_{33} = S^{c}$ and $S^{M}_{11} = S^{ab}$, but S^{M}_{13} is not determined.

The Seebeck coefficient anisotropy is moreover noted for all the measured bars, and the $\Delta S = S^{ab} - S^{c}$ gap increases with temperature (Fig. 5b). There are no similar results on bulk $Ca_3Co_4O_9$ materials in the literature, except that reported on ceramics textured by the RTG technique [10], but the authors did not comment it. However, the thermopower anisotropy has been observed in other oxides such as Ca_xCoO_2 [27], $La_{0.9}Ca_{0.1}MnO_3$ [28] and Sr_xCoO_2 [29] thin films. These results are consistent with the tensorial definition of the Seebeck coefficient, evidencing that the thermopower effect is more pronounced in the (**a**,**b**) planes than in the ones containing the mean **c***-axis.
Otherwise, the small differences between the S^{c} (T) curves may probably come from an inhomogeneity either in oxygen stoichiometry and/or in extrinsic microstructural characteristics as GBD and texture when comparing the fourth bars to each other. Further analyses are needed to precisely explain the origin of such differences.

It should be further noted that the S^{M}_{ij} values of textured bulk materials are between the ones (S_{ij}) of the single crystal and the isotropic ones of a randomly oriented bulk material. Our specimens are strongly textured with a narrow **c***-axes distribution around the pellet axis (the FWHM of the distribution is not larger than 5°) and S^{M}_{33} is

probably close to the value of the single crystal.

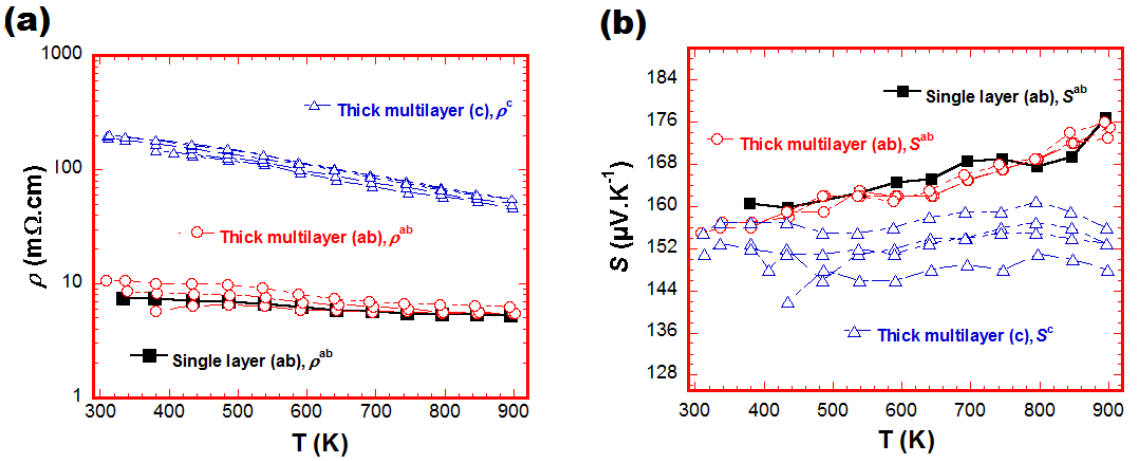

Fig. 5. Temperature dependence of (**a**) the electrical resistivity and (**b**) the Seebeck coefficient measured in the 350-900 K range, in the mean (**a**,**b**) planes (ρ^{ab},S^{ab}) and parallel to the mean **c***-axis (ρ^{c},S^{c}) of the thick multilayer sample. The corresponding ρ^{ab} and S^{ab} of the single layer sample are plotted as well.

Since S^{ab} is larger than S^{c} and ρ^{ab} much lower than ρ^{c}, the power factor PF^{ab} is much higher than PF^{c} reflecting a strong anisotropic character. PF^{c} did not exceed 46 $\mu W.m^{-1}.K^{-2}$ at 900°C whereas PF^{ab} reached 555 $\mu W.m^{-1}K^{-2}$ which is among the highest values achieved so far on undoped bulk $Ca_3Co_4O_9$ materials [9]. That led to the largest anisotropy ratio $PF^{ab}/PF^{c} = 12$ attained to date on such compounds. This value depicts a 20% increase compared to the $Ca_3Co_4O_9$ ceramics textured by RTG [10].

3.3. Thermal properties

The thermal conductivity measured in the mean (**a**,**b**) planes, κ^{ab}, and in the ones containing the mean **c***−axis, κ^{c}, of the thick multilayer sample as well as that recorded for the conventionally sintered material, κ^{CS}, decrease with temperature in the 300 − 1000 K range (Fig. 6a). κ is generally expressed by the sum of the lattice component, κ_L, and the electronic one, κ_e, ($\kappa = \kappa_L + \kappa_e$) which can be assessed by the Wiedemann-Franz law as: $\kappa_e = L.\sigma.T = L.T/\rho$, where $L = 2.45\ 10^{-8}\ V^2.K^{-2}$ is the Lorentz number [30]. κ_L is hence more dominant than κ_e in $Ca_3Co_4O_9$ materials as ρ^{ab} and ρ^{c} drop with temperature, which is evidenced in Fig. 6b. The corresponding resistivity, ρ^{CS}, of the conventionally sintered sample was reported to decrease with the temperature as well [9].

κ_L is otherwise tied to the mean free path of the phonons, l_L, by the kinetic formula: $\kappa_L = 1/3\ x\ (C_D v_L\ l_L)$, where C_D is the lattice specific heat and v_L the phonon group velocity. Decreasing κ_L can be then achieved by reducing l_L, supposing C_D and v_L unchanged. Such approach is the cornerstone of the enhancement of TE performances in nanostructuring materials owing to high phonon scattering at grain boundaries [31, 32].

For the conventional sintered sample, there is a high number of barriers (pores and grain boundaries) which fosters phonon scattering and, subsequently, reduces l_L and κ_L^{cs}. Moreover, ρ^{CS} is reported to be much larger than ρ^{ab} [9], which leads to more significant drop in κ_e^{CS}. These two factors explain the lower κ^{CS} values.

The larger κ in the thick multilayer sample is partly assigned to its higher bulk density. However, its κ^{ab} is much larger than κ^{c} because of the larger lattice component for κ^{ab} than for κ^{c} (Fig. 6b). It is, in fact, derived from the larger l_L in the (**a**,**b**) planes, as a result of phonon scattering on a lower number of grain boundaries, compared to the conduction along the mean **c***-axis. The electronic component for κ^{ab} is larger than that for κ^{c} as well, due to the lower ρ^{ab} compared with ρ^{c}. Furthermore, the anisotropic character of the $Ca_3Co_4O_9$ structure and the texture [33] were also reported to foster an increase in κ^{ab}.

The thick multilayer sample displayed κ^{ab} of 3.1 $W.m^{-1}K^{-1}$ and κ^{c} of 1.15 $W.m^{-1}K^{-1}$ at 900 K, which are 3.6 and 1.3 fold κ^{CS}, respectively. The anisotropy ratio κ^{ab}/κ^{c} reached then 2.7. The κ^{ab} value was larger than those published

for textured bulk materials by Wang *et al.* [34] (1.96 $W.m^{-1}K^{-1}$) and Zhang *et al.* [35] (1.6 $W.m^{-1}K^{-1}$). It should be noticed that most authors did not specify the direction of the thermal conductivity measurements on their samples, and Xu *et al.* [36] reported a similar κ (2.9 $W.m^{-1}K^{-1}$) to κ^{ab} at 900 K.

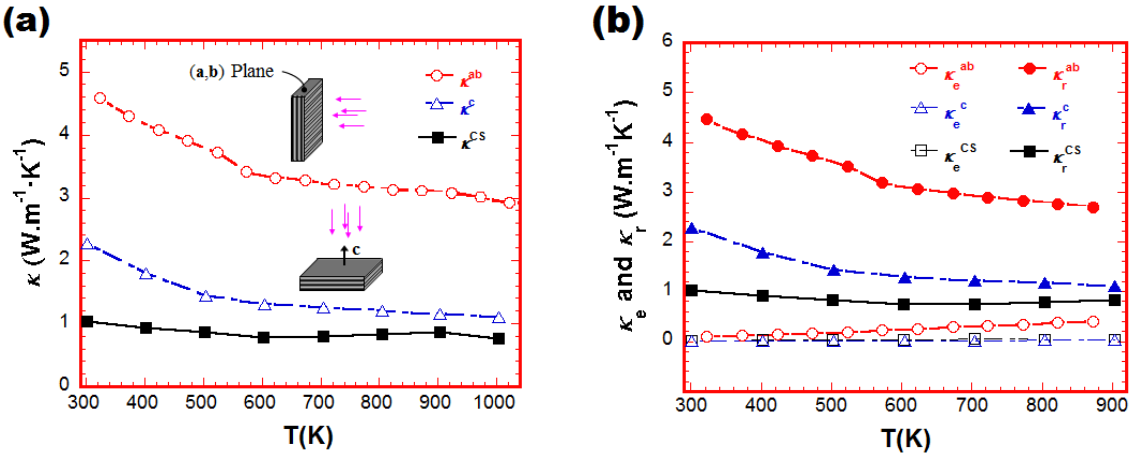

Fig. 6. (a) Temperature dependence of the thermal conductivity measured in the 300-1000 K range for the conventionally sintered sample, κ^{CS}, as well as in the mean (**a**,**b**) planes , κ^{ab}, and in the ones, κ^{c}, containing the mean **c***-axis of the thick multilayer. (**b**) Temperature dependence of the lattice component κ_L and the electronic component κ_e for κ^{CS}, κ^{ab} and κ^{c}.

3.4. Thermoelectric efficiency

The figure-of- merit, *ZT*, obtained in the mean (**a**,**b**) planes, ZT^{ab}, and parallel, ZT^{c}, to the mean **c***−axis of the thick multilayer sample, as well as for the conventionally sintered one, ZT^{CS}, monotonously increases with temperature in the 300-900K investigated range (Fig. 7), thereby emphasizing the TE efficiency stability of the $Ca_3Co_4O_9$ materials. The resulting anisotropy ratio ZT^{ab}/ZT^{c} showed a monotonous increase with temperature as well, reaching 4.6 at 900 K. ZT^{ab} was found to display the largest values and reached 0.16 at 900 K which 2 fold ZT^{CS}. A good fit of the mean $ZT^{ab}(T)$ curve is obtained using a second order polynomia: $ZT^{ab} = 0.0076868 - 4.4041 \times 10^{-5}\, T + 2.4081\, 10^{-7} \times T^2$ (Inset of Fig. 7), extrapolating a ZT^{ab} value of 0.2 at 1000 K.

It has to be noted here that despite the achievement of strongest texture in bulk $Ca_3Co_4O_9$ materials concomitant with the possibility to rigorously determine all properties required for assessing the TE efficiency in the (**a**,**b**) planes, our values remain far from the ZT^{ab} (0.87 at 973 K) reported by Shikano and Funahashi [37] on single crystals and which has not been reproduced yet.

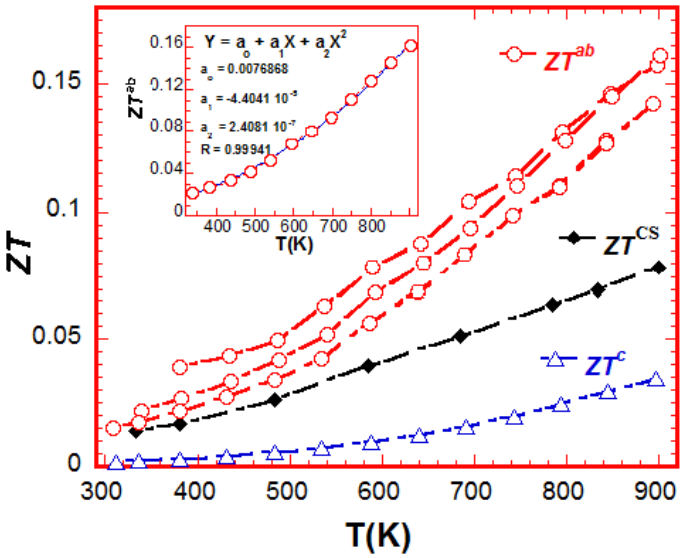

Fig. 7. Temperature dependence of the figure-of-merit, ZT, for the conventionally sintered sample, ZT^{CS}, and the thick multilayer layer in the directions parallel, ZT^{ab}, and perpendicular, ZT^{c}, to the mean **c***−axis. **Inset**: Fit of the mean ZT^{ab} (T) curves.

4. Conclusions

We have successfully fabricated a thick $Ca_3Co_4O_9$ multilayer sample by hot-pressing a stack of dense and strongly textured $Ca_3Co_4O_9$ bulk single-layer samples along their mean **c***-axis. Such material satisfies requirements of high texture strength to achieve the optimal TE performances and a large material size well-suited for TE devices fabrication. The thick sample, in particular, enabled rigorously measuring all properties required to determine the TE efficiency along two principal directions in highly textured $Ca_3Co_4O_9$ bulk oxides. Electrical and thermal properties were revealed to be anisotropic, thereby leading to strong anisotropy of the figure-of-merit, *ZT*. The latter was found of 0.16 at 900 K in the (**a**,**b**) planes and a value of 0.2 predicted at 1000 K.

Acknowledgements

Driss Kenfaui and the authors acknowledge the "Conseil Régional de Basse-Normandie, France" for the fellowship and financial participation for experimental set-up used in this work.

References

[1] J.W. Fergus, J. Eur. Ceram. Soc. 32 (2012) 525–540.
[2] K. Koumoto, I. Terasaki, R. Funahashi, Mater. Res. Soc. Bull. 31 (2006) 206–210.
[3] S. Li, R. Funahashi, I. Matsubara, K. Ueno, H. Yamada, J. Mater. Chem. 9 (1999) 1659–1660.
[4] A.C. Masset *et al*. Phys. Rev. B 62 (2000) 166–175.
[5] K. Fujita, T. Mochida, K. Nakamura, Jpn. J. Appl. Phys. (2001) 4644-4647.
[6] S. Bhattacharya *et al.* J. Cryst. Growth 277 (2005) 246-251.
[7] Y. Zhang, J. Zhang, Q. Lu, Ceram. Int. 33 (2007) 1305–1308.
[8] D. Kenfaui, M. Gomina, D. Chateigner, J. G. Noudem, Ceram. Int. 40 (2014) 10237–10246.
[9] D. Kenfaui, D. Chateigner, M. Gomina, J. G. Noudem, Int. J. Appl. Ceram. Technol. 8 (1) (2011) 214–226.
[10] T. Tani, H. Itahara, C. Xia, J. Sugiyama, J. Mater. Chem. 13 (2003) 1865–1867.
[11] H. Grimmer, Acta Cryst. A49 (1993) 763-771.
[12] D. Kenfaui, G. Bonnefont, D. Chateigner, G. Fantozzi, M. Gomina, J. G. Noudem, Mat. Res. Bull. 45 (2010) 1240-1249.
[13] J.G. Noudem, D. Kenfaui, S. Quetel-Weben, C.S. Sanmathi, R. Retoux, M. Gomina, J. Am. Ceram. Soc. 94 [8] (2011) 2608-2612
[14] D. Kenfaui, D. Chateigner, M. Gomina, J. Noudem, J. Alloys Comp. 490 (2010) 472-479.
[15] J. G. Noudem, D. Kenfaui, D. Chateigner, M. Gomina, Scr. Mater. 66 (2012) 258–260.

[16] C.H. Lim, S.-M. Choi, W.-S. Seo, H.-H. Park, J. Electron. Mater. 41 (2012) 1247-1255.
[17] S.-M. Choi, K.-H. Lee, C.-H. Lim, W.-S. Seo, Energ. Conv. Manage. 52 (2011) 335-339.
[18] E. Sudhakar Reddy, J. G. Noudem, S. Hébert, C. Goupil, J. Phys. D 38 (2005) 3751-3755.
[19] J.G. Noudem, S. Lemonnier, M. Prevel, E.S. Reddy, E. Guilmeau, C. Goupil, J. Eur. Ceram. Soc. 28 (2008) 41-48.
[20] R. Funahashi, S. Urata, Int. J. Appl. Ceram. Technol. 4 (2007) 297-307.
[21] D. Chateigner, "Combined analysis" (2010), Wiley-ISTE, New York, 496 pages.
[22] H. M. Rietveld, J Appl. Cryst. 2 (1969) 65-71.
[23] L. Lutterotti, D. Chateigner, S. Ferrari, J.Ricote, Thin Solid Films 450 (2004) 34-41
[24] L. Lutterotti, S. Matthies, H.-R. Wenk. MAUD (Material Analysis Using Diffraction): A User Friendly Java Program for Rietveld Texture Analysis and More. Textures of Materials: Proceedings of ICOTOM14. ed. J A Spunar. National Research Council of Canada, Ottawa; 1999, 1599–1604.
[25] D. Chateigner, J. Appl. Crystallogr. 38 (2005) 603-611.
[26] J.F. Nye, Physical properties of crystals: their representation by tensors and matrices, Lavoisier 1985.
[27] T. Kanno, S. Yotsuhashi, H. Adachi, Appl. Phys. Lett. 85 (2004) 739-742.
[28] L. Yu, Y.Wang, P.X. Zhang, H.-U.Habermeier, J. Cryst. Growth. 322 (2011) 41–44.
[29] A.Sakai, T.Kanno, S.Yotsuhashi, S.Okada, H.Adachi, J. Appl. Phys. 99 (2006) 093704-093707.
[30] M. E. Fine, N. Hsieh, J. Am. Ceram. Soc. 57 (1974) 502-503.
[31] B. Poudel, Q. Hao, Y. Ma, Y. Lan, A. Minnich, B. Yu *et al*. Science, 2008, 320, 634–638.
[32] Q. Lognone, F. Gascoin, O. I. Lebedev, L. Lutterotti, S. Gascoin, D. Chateigner. J. Am. Ceram. Soc. **97(7)**, 2014, 2038-2045
[33] M. Mikami, E. Guilmeau, R. Funahashi, K. Chong, D. Chateigner, J. Mat. Res. 20(9) (2005)2491–2497.
[34] D. Wang, L. Chen, Q. Wang, J. Li, J. Alloy Compd. 376 (2004) 58-61.
[35] Y. Zhang, J. Zhang, J. mater. Proc. Technol. 208 (2008) 70-74.
[36] G. Xu, R. Funahashi, M. Shikano, Q. Pu, B. Liu, Solid State Comm. 124 (2002) 73-76.
[37] M. Shikano, R. Funahashi, Appl. Phys. Lett. 82 (2003) 1851–1853.